HHS Public Access

Author manuscript

Bone. Author manuscript; available in PMC 2021 February 01.

Published in final edited form as:

Bone. 2020 February ; 131: 115078. doi:10.1016/j.bone.2019.115078.

Perlecan/*Hspg2* deficiency impairs bone's calcium signaling and associated transcriptome in response to mechanical loading

Shaopeng Pei[1], **Sucharitha Parthasarathy**[2], **Ashutosh Parajuli**[3], **Jerahme Martinez**[1], **Mengxi Lv**[1], **Sida Jiang**[1], **Danielle Wu**[4], **Shuo Wei**[2], **X. Lucas Lu**[1], **Mary C. Farach-Carson**[4], **Catherine B. Kirn-Safran**[2,5], **Liyun Wang**[1,2,3,*]

[1]Center for Biomechanical Engineering Research, Department of Mechanical Engineering, University of Delaware, Newark, DE 19716

[2]Department of Biological Sciences, University of Delaware, Newark, DE 19716

[3]Department of Biomedical Engineering, University of Delaware, Newark, DE 19716

[4]Department of Diagnostic and Biomedical Sciences, School of Dentistry, University of Texas Health Science Center, Houston, TX 77054

[5]Department of Biology, Widener University, Chester, PA 19013

Abstract

Perlecan, a heparan sulfate proteoglycan, acts as a mechanical sensor for bone to detect external loading. Deficiency of perlecan increases the risk of osteoporosis in patients with Schwartz-Jampel Syndrome (SJS) and attenuates loading-induced bone formation in perlecan deficient mice (Hypo). Considering that intracellular calcium $[Ca^{2+}]_i$ is an ubiquitous messenger controlling numerous cellular processes including mechanotransduction, we hypothesized that perlecan deficiency impairs bone's calcium signaling in response to loading. To test this, we performed real-time $[Ca^{2+}]_i$ imaging on *in situ* osteocytes of adult murine tibiae under cyclic loading (8N). Relative to wild type (WT), Hypo osteocytes showed decreases in the overall $[Ca^{2+}]_i$ response rate (−58%), calcium peaks (−33%), cells with multiple peaks (−53%), peak magnitude (−6.8%), and recovery speed to baseline (−23%). RNA sequencing and pathway analysis of tibiae from mice subjected to

*Corresponding author: Liyun Wang, Ph.D., Center for Biomedical Engineering Research, Department of Mechanical Engineering, University of Delaware, Newark, DE 19711, 302-453-8372 (office), lywang@udel.edu.

Author Contributions Statement

Study design: XLL, CKS, MCFC, LW; data collection: S Pei, S Parthasarathy, AP, JM, ML; data analysis: S Pei, ML, SJ, SW, XLL, CKS, MCFC, LW; manuscript writing: S Pei, JM, XLL, CKS, MCFC, LW. LW and MCFC designed the experiments and secured the funding. All authors reviewed the results and approved the final version of the manuscript.

Conflict of Interests

The authors declare no conflict of interests.

Data Availability

RNA sequencing datasets are available in supplementary files and will be uploaded to NCBI after this work is accepted for publication.

Supplementary Information

Supplemental materials include 2 figures, 5 tables, and 1 movie.

one or seven days of unilateral loading demonstrated that perlecan deficiency significantly suppressed the calcium signaling, ECM-receptor interaction, and focal adhesion pathways following repetitive loading. Defects in the endoplasmic reticulum (ER) calcium cycling regulators such as *Ryr1*/ryanodine receptors and *Atp2a1*/Serca1 calcium pumps were identified in Hypo bones. Taken together, impaired calcium signaling may contribute to bone's reduced anabolic response to loading, underlying the osteoporosis risk for the SJS patients.

Keywords

perlecan; Schwartz-Jampel Syndrome (SJS); osteocyte; tibial loading; intracellular calcium; ER calcium regulators

1. Introduction

Perlecan, a heparan sulfate proteoglycan encoded by the *Hspg2* gene, is one of the largest (~200 nm contour length) and oldest (> 550 million years) extracellular matrix (ECM) molecules [1]. Consisting of five globular domains (470 kDa) and 3 or 4 attached glycosaminoglycan (GAG) side chains (each ~70–100 kDa) [2], perlecan is found mostly in the basement membrane and the territorial matrix of skeletal muscle and bone [1]. Through its core protein and GAG side chains, perlecan interacts with many cell surface receptors (*e.g.,* integrins, vascular endothelial growth factor receptors, semaphorins), the other ECM molecules (*e.g.,* laminin and collagens), and growth factors (*e.g.,* fibroblastic growth factors) [3,4]. These properties allow perlecan to function as matrix scaffold, growth factor depot [3], and barrier molecule at tissue borders including the osteocytic pericellular matrix within the lacunar-canalicular system (LCS) [5]. As perlecan plays critical roles in tissue development and matrix maintenance, global knockout of perlecan is developmentally lethal (due to cardiovascular defects and other gross deformities) while deficiency of perlecan produces myopathies, ocular abnormalities, and profound skeletal disorders including Schwartz-Jampel Syndrome (SJS, OMIM entry 255800) [6,7]. SJS patients are prone to bone/cartilage loss, and perlecan deficiency is a risk factor for osteoporosis [8].

The exact molecular mechanisms by which perlecan deficiency leads to an osteoporotic phenotype have not been elucidated fully. Previous studies attributed the phenotype mainly to impaired endochondral ossification, accelerated mineralization, and increased tissue brittleness [9]. Recently, bones from perlecan deficient mice were found to display impaired responses to physiological mechanical stimuli [10], in contrast to normal healthy bone, which is sensitive to its mechanical environment [11]. Detailed microstructural imaging and functional analysis from our previous work demonstrated that perlecan is present around osteocytes within healthy bone, and that deficiency of perlecan accelerates mineralization [9] and narrows the LCS channels [5], the major conduits for mature osteocytes to obtain nutrients and communicate with other cells [12,13]. Our recent single-molecule study showed that the perlecan core protein is long (~200 nm) and strong (~71 MPa) enough [14] to span the pericellular space in the LCS and forms the tethers, which were originally visualized by You et al. (2004) [15] and postulated to help osteocytes sense load-induced fluid flow [16]. The reduced number of these tethering sensors and the overall reduction in

the fluid force experienced by osteocytes might have contributed to the diminished load-induced bone formation in perlecan deficient mice under normally anabolic tibial loading [10]. Furthermore, perlecan is widely distributed in bone marrow [1], and marrow plays important roles in bone adaptation. Previous studies have clearly shown that mechanical stimulation of bone marrow through intramedullary pressurization [17,18] or muscle contraction [19] could drive bone adaptation *in vivo*. Interestingly, this effect was present even when osteocytes signaling was attenuated *in vivo* [20] or blocked *in vitro* [21]. At the cellular level, deformation of trabecular bone was shown to subject local bone marrow and the residing cells to shear stress and hydraulic pressure [22]. Application of these stimulations *in vitro* was found to regulate the function and signaling of marrow-residing cells such as stromal osteoblast progenitors [23], preosteoclasts [24], and hematopoietic progenitor cells [25].

Despite these recent advances, less is known regarding bone's downstream mechanotransduction pathways affected by perlecan deficiency. Because perlecan is strategically positioned in the osteocytic pericellular matrix [5], the frontier interface between the cells and their immediate environment [1,3], we hypothesized that perlecan deficiency alters the "outside-in" signaling pathways and impairs the cellular responses to mechanical loading. *In vitro* and *in vivo* studies (reviewed previously [26–28]) have identified several signaling pathways involving cell-surface components that can sense and respond to external loading. These include the ECM-receptor interaction [29,30], focal adhesion [30], PI3k-Akt [31], Wnt/β-catenin [32], and calcium signaling pathways [33,34]. Upon mechanical stimulation, bone cells, including osteoblasts, osteocytes, and mesenchymal bone marrow progenitor cells, all display transient oscillation of intracellular calcium concentration $[Ca^{2+}]_i$ [33–37]. Being an ubiquitous second messenger, the intracellular calcium in the cytoplasm and the endoplasmic reticulum (ER) controls numerous cellular activities [38]. Therefore, we further hypothesized that perlecan deficiency impairs the intracellular calcium signaling in bone and the encased osteocytes during mechanical loading.

In this study, we used the SJS-mimicking, perlecan deficiency (termed Hypo) mouse model [6] to test our hypothesis at the molecular, cellular, and tissue levels. First, a newly developed *ex vivo* confocal imaging technique [34] was used to study the effects of perlecan deficiency on loading-induced $[Ca^{2+}]_i$ responses inside osteocytes of WT and Hypo bones *in situ*. We then subjected young adult mice to unilateral tibial loading for a short (one day) or a relatively longer (seven days) duration, and analyzed their tibiae for transcriptome changes and signaling pathway enrichment using RNA sequencing as performed previously on bone tissues [29]. High-throughput RNA sequencing allows unbiased profiling of the gene products associated with various bone phenotypes [39]. These investigations aimed to elucidate the pathways through which perlecan regulates bone's adaptive response to mechanical loading that leads to new bone formation.

2. Methods

2.1. Animals

Mice with perlecan deficiency (Hypo), a gift from Dr. Kathryn Rodgers [6], were crossed into the C57BL/6J background [9]. Adult 19-week-old Hypo and wild type (WT) C57BL/6 male mice were used in consistency with our previous studies [10] due to sex differences shown in Hypo skeletons [9]. The Institutional Animal Care and Use Committee (IACUC) of the University of Delaware approved all animal protocols.

2.2. Intracellular calcium imaging of osteocytes in intact tibiae

Sample preparation: Real-time osteocyte $[Ca^{2+}]_i$ responses were imaged in cyclically loaded tibiae from 8 WT and 4 Hypo mice as previously described [34]. Both tibiae were dissected and cleaned of soft tissues. After 90 min incubation in α-MEM supplemented with 5% v/v FBS/CS, and 1% v/v P/S (Hyclone Laboratories Inc., USA), bones were immersed for 30 min in α-MEM supplemented with 18 μM Fluo-8 AM (ABD Bioquest, USA) and 5% v/v charcoal-stripped FBS. Samples were washed for 10 min in α -MEM with 5% CS/FBS before fluorescent imaging.

Synchronized imaging/loading: The tibia was mounted axially between the actuator and bracket of an Electroforce® LM0 TestBench loading device (DE, USA), while the region of interest containing osteocytes embedded in mineralized matrix (~ 20 to 30 μm below the anterior-medial surface) was imaged with a water-dipping objective (20x/NA1.0, W Achroplan) of a confocal microscope (Zeiss LSM 510, Carl Zeiss, Inc., Fig. 1A). Imaging and loading were synchronized via trigger signals between the two devices as detailed previously [10,34,40]. The tibia was pre-conditioned (100–120 cycles of compressive load of 8N at 4Hz to eliminate creeping), and rested for 8 min prior to imaging. The experimental settings included 488 nm excitation, 512 × 512 pixel, 1.24 μm/pixel, open pinhole, 20 frames of baseline (no loading), and 80 frames taken during the resting periods (2.34 sec) between the cycles of loading (8N, 3 sec per cycle). From the 8 WT and 4 Hypo mice, 11 WT and 8 Hypo tibiae yielded high-quality images for analysis.

Data and statistical analysis: The images were corrected with rigid-motion artifacts (if there is any) using ImageJ (National Institute of Health, USA). The traces of $[Ca^{2+}]_i$ intensity in individual osteocytes were obtained and normalized with baseline as previously described [33] (Fig. 1A). A cell was defined as responsive if its normalized peak magnitude was larger than 1.2, four times higher than the baseline fluctuations (< 5%). Overall response parameters (percentage of responsive cells per test, average number of peaks per responsive cell and percentage of responsive cells with multiple peaks over all responsive cells) were quantified [33]. Peak dynamic parameters including peak magnitude, rising time, and recovery time (time for the $[Ca^{2+}]_i$ level to drop 50% from the peak) were acquired for the first peak immediately after loading as well as all the following peaks if there are any. Data were shown as mean ± standard deviation. Normality of each measurement was checked using the Kolmogorov-Smimov test. Student t and Mann-Whitney U tests were used to compare the percentage of responsive cells (with normal distribution) and the other measures (without normal distribution), respectively, between WT and Hypo. The Chi-

square test was used to compare the percentage of responsive cells with multiple peaks between WT and Hypo. Origin (OriginLab, USA) was used for these tests and significance was defined as $p < 0.05$.

2.3. Intracellular calcium imaging of MSCs under fluid shear

To test if perlecan deficiency affects the $[Ca^{2+}]_i$ response of other bone cells under loading, we harvested mesenchymal stromal cells (MSCs) from long bone marrow of adult WT and Hypo mice (3 mice/group). 1.3×10^5 cells were seeded on a glass slide, dyed with Fluo-8AM, exposed to 12 dyn/cm^2 fluid shear stress in a flow chamber, and the resulted $[Ca^{2+}]_i$ spikes were recorded for 10 min and analyzed as described previously [33]. Approximately 100 cells in total were examined in duplicated tests for each group.

2.4. In vivo loading experiments

Uniaxial tibial loading: For one-day loading, Hypo (n = 6) and WT (n = 10) male mice were subjected to one bout of loading (8.5 N, 4 Hz, triangle waveform with 0.1s resting, 1200 cycles) on the left tibia using an Electroforce® LM1 TestBench (DE, USA) as described [10]. The contralateral right limbs served as non-loaded controls. Strain resulted from the loading was measured to be ~1200 με by strain gauges attached on the anterior-medial surface 30% distal from the proximal end of both WT and Hypo tibiae. The applied strain level falls in the range of physiological strains associated with uphill zigzag running for humans [41]. For seven-day loading, Hypo (n = 4) and WT (n = 5) mice were loaded one bout per day for seven consecutive days. Mice were euthanized 24 hours post-loading with anesthesia overdose and cervical dislocation.

RNA extraction: Tibiae were dissected, cleansed of soft tissues, flash-frozen, and pulverized in liquid nitrogen within 10 min after sacrifice. Total RNA was isolated using the TRIzol® Reagent (Thermo Fisher Scientific, USA) and RNeasy® Mini kit (Qiagen, USA), yielding 30 μL RNA-enriched nucleic acid mixture per bone, with an average concentration of 355 ±120 ng/μL and 260/280 absorbance ratios (1.9–2.15) measured by a spectrophotometer (NanoDrop Technologies, USA). The nucleic acid extracts were cleaned of genomic DNA contamination using the TURBO DNA-Free™ kit (Ambion, Thermo Fisher Scientific), and stored in −80 °C.

RT-qPCR Validation: Aliquots of the RNA samples were reverse transcribed to 500 ng cDNA (20 μL) using iScript cDNA™ synthesis kit (Bio-Rad Laboratories, USA). Analyzed gene products (listed in Supplemental Table 1S) included those related to bone cell activities, matrix synthesis, catabolic activities, and calcium ER regulators. Quantitative PCR were performed using Power SYBR® Green PCR Master Mix on an Applied Biosystems Quantstudio 3 machine. Transcript fold-changes (F.C.) were calculated as $2^{-\Delta\Delta Ct}$ (Δ: differential value, Ct: cycle threshold, housekeeping gene: *Gapdh*) for comparing the effects of loading (loaded vs. non-loaded) and genotype (Hypo vs. WT).

RNA Sequencing: A subset of the RNA samples (6 Hypo, 6 WT, all with paired loaded and non-loaded tibiae) were submitted to UD Sequencing and Genotyping Core, following published protocol [29]. RNA quality was confirmed (integrity number: 7.9±0.9, range: 6.1–

9.8) with a fragment analyzer (Advanced Analytical Technologies, USA). Illumina-compatible barcoded libraries were prepared using Illumina® TruSeq Stranded mRNA Library Prep Kit (Illumina, USA). The 24 individually barcoded libraries were normalized and pooled at equimolar concentrations and the multiplex pool was sequenced over 3 lanes on an Illumina® HiSeq 2500 at 51 cycles single-read sequencing and a read depth of 25 million reads per sample.

Differentially expressed transcripts (DETs) were identified using accepted analytics [29,39]. FASTQ files were imported into CLC genomics workbench (Qiagen, USA) for trimming off adaptor sequences and quality control, followed by mapping to the *mus musculus* genome annotations (GRCm38.88, Ensembl). In our dataset, 96% of the reads were mapped and 80% of them mapped uniquely. DET analysis were performed using the EdgeR® package (RStudio, USA) [42], where low numbers of transcripts (zero reads per million in at least one sample) were excluded. We used "loading" as the blocking factor for loaded vs. non-loaded comparisons, and "genotype" as the blocking factor for Hypo vs. WT comparisons. The DETs were identified using a generalized linear model and likelihood ratio tests with stringent cutoff criteria of false discovery rate (FDR< 5%) and absolute >2-fold-change ($|\log_2 F.C.|>1$).

Enriched pathway analysis: The DETs were imported into the Database for Annotation, Visualization and Integrated Discovery (DAVID version 6.8, https://david.nciF.C.rf.gov/tools.jsp), from which enriched Kyoto Encyclopedia of Genes and Genomes (KEGG) pathways were further identified (Benjamini $p < 0.05$) [43,44]. For enriched pathways relevant to bone mechanotransduction, a heat map was generated by cross-referencing the DETs and the individual genes encoding the products in those pathways published on the KEGG website (https://www.genome.jp/kegg/pathway.html, version 87.0). Each row of the heat map represented one gene product within a particular pathway and each column for one comparison condition. KEGG Mapper (https://www.genome.jp/kegg/tool/map_pathway2.html, version 3.1) was used to visualize the gene network with node color indicating the increased (red) or decreased (green) levels of each gene product. For a node representing multiple genes, the color was assigned by whether more gene transcripts were increased or decreased in the RNA pool.

3. Results

3.1. Perlecan deficiency impairs the intracellular calcium signaling in bone cells

Osteocytes, the major mechano-sensors in bone, are anticipated to show more robust intracellular calcium response to loading in WT than in Hypo bones. Using the rest-inserted loading/imaging protocol developed previously [10,34,40], we acquired time series of fluorescent images of *in situ* intracellular calcium levels in osteocytes of mechanically loaded murine tibiae (Fig. 1A). The $[Ca^{2+}]_i$ traces in the representative images showed more robust $[Ca^{2+}]_i$ responses to loading in WT than Hypo (Fig. 1A). Representative recordings of $[Ca^{2+}]_i$ responses to loading in osteocytes of WT and Hypo tibiae can be found in the Supplemental Materials published online (Supplemental Movie 1). In agreement with a previous study [34], no spontaneous calcium response was observed in osteocytes during the

resting non-loaded periods (Fig. 1A, Supplemental Movie 1). The spatiotemporal characteristics of the calcium peaks were then quantified using our custom MATLAB program [33]. The number of osteocytes (186 ± 38 cells, a range of 108–249 cells) captured within the imaging field (635 μm × 635 μm) per test did not differ between Hypo and WT groups (n = 11/8 WT/Hypo tibiae). On average, 6.6% of total osteocytes responded with at least one $[Ca^{2+}]_i$ peak for Hypo tibiae, which was significantly lower (−58%) than the 15.7% responsive rate for WT tibiae ($p = 0.04$). For all the responding osteocytes (310/88 WT/Hypo cells), the average number of peaks per cell were lower in Hypo than WT (1.58 ± 1.32 vs. 2.36 ± 1.91, − 33%, $p = 5\times10^{-6}$), and the percentage of those showing multiple peaks was 2 times smaller in Hypo than in WT (25% vs. 53%, $p = 3\times10^{-6}$, Fig. 1B). The dynamic measures of the first peaks in Hypo, relative to WT, showed a trend of lower peak magnitude (1.41 ± 0.23 vs. 1.49 ± 0.36, −5.4%, $p = 0.09$), longer rising time (8.70 ± 4.15 sec vs. 7.88 ± 4.16 sec, +10.4%, $p = 0.04$, and longer recovery time (7.15 ± 5.46 sec vs. 5.34 ± 4.02 sec, +33.9%, $p = 0.0004$, Fig. 1C). Pooling all peaks together, similar changing patterns were observed in Hypo relative to WT in the peak magnitude (−6.8%, $p = 0.001$) and relaxation time (+23%, $p = 0.0007$), but no change in rising time (+0.4%, $p = 0.5$, Fig. 1D). In summary, the $[Ca^{2+}]_i$ response in the loaded Hypo bone was impaired, as shown with significantly fewer responsive cells, lower peak magnitude, longer peak rising time, and delayed recovery to baseline from the peak (Fig. 1).

We also tested if the observed impairment of intracellular calcium signaling is present in osteogenic progenitor cells. We harvested bone marrow from the WT and Hypo mice (n = 3 mice) to obtain primary mesenchymal stromal cells (MSCs, Fig. 2A). When subjected to 1 Pa fluid shear stimulation in a parallel-plate flow chamber as we reported previously [33], fewer Hypo MSCs showed calcium peaks than WT cells (Fig. 2B), leading to an approximate 3-fold decrease in the responsive rate (0.088) relative to WT (0.28, Fig. 2C). The robust calcium response seen in MSC derived from WT bone marrow provides additional support that bone marrow and its residing cells are mechanoresponsive as demonstrated previously [17,18,23–25].

3.2. Perlecan deficiency suppresses the transcripts of ER calcium regulators in mechanically loaded bone

Both the *in situ* and *in vitro* $[Ca^{2+}]_i$ recordings suggested the impairment of bone's intracellular calcium signaling process [45] associated with the perlecan deficiency. We thus investigated whether the transcripts of calcium signaling pathway (KEGG 04020) were altered in mechanically loaded Hypo bones compared with WT. The total RNA samples after 1-day or 7-day tibial loading were subjected to unbiased sequencing, from which the differentially expressed transcripts (DETs) of the calcium signaling pathway induced by loading or perlecan deficiency were obtained. Comparing loaded vs. non-loaded tibiae, both WT and Hypo mice showed increased levels (red color, fold changes > 1) of the transcripts annotated in the calcium signaling pathway (Fig. 3A, left panels). In contrast, when comparing Hypo vs. WT six or seven transcripts of the calcium signaling pathway showed decreased levels (green color, fold changes < 1, Fig. 3A; right panels). Transcripts that did not pass the cut-off of false discovery rate (FDR < 0.05) are indicated by black color. We further performed the enrichment analysis for the calcium signaling pathway using DETs

with a fold-change above 2 or below 0.5, and FDR ≤ 0.05. It was found that the pathway was significantly enriched in 7-day Hypo loaded samples relative to WT (Benjamini $p = 0.006$, Fig. 3A), with all 7 DETs showed decreased expression (green color, Fig. 3B) and their fold-changes in the range of 0.12–0.26 (Fig. 3C). The transcript levels were reduced for the two key regulators of the ER calcium dynamics, sarco/endoplasmic reticulum Ca^{2+}-ATPase 1 (*Atp2a1*) involved in refilling ER calcium stores, and the ryanodine receptor 1 (*Ryr1*) involved in releasing calcium from the ER stores [38,46]. The finding was further corroborated using real-time quantitative PCR (fold-change < 1, Fig. 3D). Taken together, these results indicated that perlecan deficiency is associated with suppressed *Atp2a1* and *Ryr1*, which may have led to the observed impairment of $[Ca^{2+}]_i$ responses of bone cells to mechanical loading in Hypo bones (Figs. 1 and 2).

3.3. Repetitive 7-day loading induces more DETs and enriched “outside-in” signaling pathways than 1-day loading

The above findings on the intracellular calcium signaling, one of the “outside-in” signaling pathways, motivated us to examine four other related mechanotransduction pathways (ECM-receptor interaction [29,30], focal adhesion [30], PI3k-Akt [31], and Wnt/β-catenin [32]). Both WT and Hypo tibiae responded to 1-day loading in terms of the numbers of DETs (WT: 39 and Hypo: 15, Fig. 4A), but none of the four pathways were significantly enriched by loading in either genotype (Fig. 4C). 7-day repetitive loading led to more wide-spread transcriptome changes, with approximately 10/30 times more DETs in WT/Hypo bones (WT: 368 and Hypo: 439, Fig. 4B). In contrast to 1-day loading where only one third of the DETs showed increase (Fig. 4A), the expression of nearly all DETs increased in the 7-day loaded tibiae regardless of the genotype (Fig. 4B). Interestingly, some of these DETs were not found in both genotypes (103 transcripts unique to WT vs. 174 transcripts unique to Hypo). Furthermore, three out of the four examined pathways (ECM-receptor interaction, focal adhesion, and PI3k-Akt) showed an extremely high significance level for enrichment (Benjamini p value on the order of 10^{-10} to 10^{-23}) with the number of DETs varying from 25 to 35 per pathway (Fig. 4C). A full list of loading-induced DETs and detailed KEGG pathway enrichment analysis can be found in Supplemental Table 2S.

3.4. Perlecan deficiency alters the transcriptome profiles and suppresses selective “outside-in” signaling pathways

Relative to the WT, Hypo mice demonstrated markedly different transcriptome profiles as shown with the large numbers of DETs in either 1-day groups (92/126 DETs, Fig. 5A) or 7-day groups (164/121 DETs, Fig. 5B). Similar to the calcium signaling pathway, suppression of the ECM-receptor interaction and focal adhesion pathways by perlecan deficiency was found in the 1-day loaded group, with the suppression of the latter being persistent in the 7-day groups (Fig. 5C). Detailed inhibitory effects (green) on individual genes/gene groups were shown for the ECM-receptor interaction and focal adhesion pathways (Figs. 5D and 5E). The suppressed ECM-receptor interaction pathway after 1-day loading was mainly due to the decreased transcripts encoding ECM molecules (collagen, fibronectin, and perlecan) and integrin (green boxes, Fig. 5D). For the focal adhesion pathway, besides the reduced levels of transcripts encoding ECM, decreased levels were seen for the transcripts of genes encoding actin (MLC box) and downstream myosin kinases (MLCK box) in the Hypo bones

after 7-day loadings (7D HL/WL, Fig. 5E). The full list of DETs (Hypo vs. WT) and detailed pathway enrichment analysis can be found in the Supplemental Table 3S.

3.5. Perlecan deficiency blunts the activation of signaling pathways induced by loading

To illustrate the overall effects of loading and perlecan deficiency on bone's transcriptome profiles, a heat map was constructed for the five signaling pathways as well as the hedgehog and TGF-beta signaling pathways (due to their roles in skeletal development and bone adaption) (Fig. 6). Among all 8 comparisons to evaluate the effects of loading or genotype (significance is indicated with * $p < 0.05$ and ** $p < 0.01$, Fig. 6), the most frequently enriched pathway was focal adhesion pathway (5 times), followed by the ECM-receptor interaction pathway (3 times), PI3K-Akt signaling pathway (2 times), and calcium signaling pathway (1 time). Overall, mechanical loading resulted in mostly elevated expression of transcripts with $|\mathrm{Log}_2(\text{fold-change})| > 1$ in these pathways regardless of genotype (the red colored lines in the left four columns, Fig. 6); in contrast, decreased expression of transcripts were found in the Hypo bones compared with WT, especially for the transcripts in the ECM-receptor interaction, focal adhesion, and calcium signaling pathways (the green colored lines in the right four columns, Fig. 6). The full list of genes associated with these pathways and their fold-changes can be found in the Supplemental Table 4S.

4. Discussion

The findings from the present study support our hypothesis that perlecan deficiency alters bone's calcium signaling and the associated mechanotransduction pathways, which may contribute to the diminished loading-induced bone formation in Hypo mice [10] and the increased risk of osteoporosis observed in SJS patients [8]. Our direct *in situ* measurements of the $[Ca^{2+}]_i$ response of bone cells to loading clearly demonstrated bone's impaired calcium signaling due to perlecan deficiency, as the Hypo bones showed fewer responsive cells, lower calcium peak magnitude, and delayed return to baseline from the peak. Furthermore, our RNA sequencing and pathway analysis revealed an overall suppression of the calcium signaling pathway in the perlecan deficient bones following mechanical loading. Previously we found that perlecan binds to and co-localizes with the $\alpha_2\delta_1$subunit of the voltage sensitive calcium channels and that magnetically twisting of the $\alpha_2\delta_1$ subunit results in calcium influx in cultured osteocytes *in vitro* [47]. Therefore, when mechanical loading induces fluid flow in the osteocytic LCS [10,14], the fluid flow can stretch the pericellular perlecan tethers [5], and further activate calcium ion channels via interacting with the channels' $\alpha_2\delta_1$ subunits. The resulting initial calcium influx, in turn, may lead to the calcium release from ER calcium store through the activation of ER calcium cycling regulators *Ryr1* and *Atp2a1* [38,46]. This hypothetical scenario is consistent with many *in vitro* and *in situ* calcium signaling studies. When osteocytes were subjected to mechanical stimulation, blocking the initial calcium influx by removing extracellular calcium source or using ion channel inhibitors [33,48] led to the reduction or total abolishment of the intracellular calcium peaks, as did with the depletion of the ER calcium stores [34]. The findings from the present study provide convincing evidence that perlecan plays an important role in bone's $[Ca^{2+}]_i$ responses to mechanical stimulation, one of the earliest molecular events under loading that leads to osteogenesis [26,33,49].

The detrimental effect of perlecan deficiency on the transcripts of intracellular ER calcium regulators is a novel finding in this study. To our best knowledge, there is no report of direct interactions between perlecan and Ryr1/ryanodine receptors or Serca1/ATPase calcium pumps in bone cells. However, heparan sulfate, the major component of perlecan side-chains, is suggested to modulate the calcium kinetics within muscle, by binding and regulating the activity of ion channels such as the dihydropyridine receptor [50–52], and the ryanodine receptor [53,54] on the sarcoplasmic reticulum membrane. Deficiency of heparan sulfate in primary myofibers significantly decreased the amplitude of electrically induced calcium peaks and a slower removal of cytosolic calcium ions [55]. The mechanisms by which pericellular perlecan around osteocytes regulates the gene expression and function of ER ryanodine receptors and Serca calcium pumps remain to be determined. It is also possible that the observed effect might be due to interactions between the intracellular fraction of perlecan and the ER calcium regulators, similarly to what was suggested in muscle sarcoplasmic reticulum [55].

To explore perlecan's potential interacting partners, we asked if there exist transcripts of membrane/surface proteins implicated in mechanotransduction that exhibit change patterns similar to that of the perlecan-encoding transcript of *Hspg2*. Taking advantage of our large data set of transcriptome profiles under the experimental conditions (2 genotypes × 2 loading conditions × 2 loading durations), we calculated and ranked the Pearson correlation coefficients between the DETs and *Hspg2*. We found 24 transcripts with a correlation coefficient > 0.70 (Supplemental Table 5S). The highest correlated transcript to *Hspg2* is *Cacna1c* that encodes the L-type calcium channel pore forming unit (correlation: 0.94), which can be found in hematopoietic stromal cells, osteoblasts, and osteocytes (to a lesser degree) [56,57]. The list also contains accessory voltage-gated channel subunits such as *Cacnb3* (0.87), *Cacng7* (0.84), and ion channels previously described as mechanosensors such as *Piezo2* (0.84) [58] and *Trpv4* (0.84) [59]. Future investigation is needed to confirm if perlecan interacts with these targets and if the disruption of these interactions affects downstream calcium signaling in bone.

The effects of perlecan deficiency on other related mechanotransduction signaling pathways were thoroughly examined in this study following 1- or 7-day loading. The finding that 7-day repetitive loading results in more robust transcriptome changes than the 1-day loading was consistent with previous observations in female rats [60] and in mouse vertebral trabecular osteocytes [61]. In agreement with literature [27,28], the ECM-receptor interaction, focal adhesion, and PI3K-Akt pathways were significantly enriched in wild type bones after 7-day loading. In contrast, the first two pathways were suppressed in the perlecan deficient bones. Considering perlecan's accepted role in maintaining matrix integrity by scaffolding ECM molecules and mediating cell-substratum interactions, the destabilization of pathways associated with ECM-receptor and focal adhesion in Hypo mice comes as no surprise. Because mechanical stimulation is a potent anabolic factor for osteogenesis and for bone maintenance [11–13], the impairment of these mechanotransduction pathways may contribute, at least partially, to the reduced bone formation found in perlecan deficient mice [10] as well as the increased osteoporosis risk in SJS patients [8].

The present study has several limitations. Although our results of *in situ* intracellular calcium imaging corroborated the RNA sequencing finding of suppressed calcium signaling pathway in perlecan deficiency, activities of other enriched signaling pathways (*e.g.*, ECM-receptor interaction and focal adhesion) require further validation at the protein and function levels. However, the confidence on our RNA sequencing data was reasonably high, as the representative transcripts related to matrix production, cellular activities, and matrix degradation were found to correlate well with data obtained from RT-qPCR (Supplemental Fig. 1S). Furthermore, this study used RNA samples from whole mouse bone tissues, unlike previous studies using marrow-free cortical and trabecular bone [29], primary trabecular osteocytes [61], or MLO-Y4 osteocyte cell line [62]. Although our sample preparation allowed the study of the contribution of marrow to bone's loading response as suggested previously [21], the results from the present study should be compared to literature data with this difference in mind. The Wnt/beta-catenin signaling pathway, for example, was found to be enhanced after a single bout of loading in marrow-free RNA samples [29], but not in the present study. However, the fold-changes for differentially expressed transcripts were comparable between these two studies (Supplemental Fig. 2S). Nevertheless, future work using osteocyte-enriched samples could provide more definitive information regarding the effect of perlecan deficiency on the Wnt/beta-catenin signaling pathway. It is also noted that, while this study failed to detect change of SOST transcripts in WT tibiae after loading, previous studies using the ulnar loading model [63–65] reported decreased mRNA and protein expression levels of SOST/sclerostin. This discrepancy was likely due to the different loading magnitudes applied to the bone: high surface strains (~2200 to 3240 με) in those studies vs. a moderate level of strain (~1200 με) in this study. We had to limit the load magnitude (8.5 N) because larger loads were found to damage the knee joints [66,67]. Studies that aim at testing if bone exhibits dose-dependent transcriptome responses within a larger range of mechanical strains would need to be conducted using the ulnar model. In this study, however, we chose the tibial loading model because it was better suited for in situ imaging of osteocytes in loaded bones.

Despite its limitations, the present study clearly demonstrated that perlecan deficiency impairs the calcium signaling and the associated transcripts following repetitive loading of the skeleton. The defective calcium signaling, coupled with altered ECM-receptor interaction and focal adhesion pathways, could contribute to the diminished osteogenesis in perlecan deficient mice and the increased risk of osteoporosis in SJS patients.

Supplementary Material

Refer to Web version on PubMed Central for supplementary material.

Acknowledgements

The study was supported by NIH grants (P30GM103333, R01AR054385). The RNA sequencing work was supported partially by a core access award through NIH NIGMS IDeA Program grant (P20GM103446). We acknowledge the excellent consulting and technical support from Dr. Brewster Kingham, Director of UD's DNA Sequencing & Genotyping Center, and helpful discussion with Dr. Jian Wang from the University of Delaware.

References:

[1]. Farach-Carson MC, Warren CR, Harrington D. a., Carson DD, Border patrol: insights into the unique role of perlecan/heparan sulfate proteoglycan 2 at cell and tissue borders., Matrix Biol 34 (2014) 64–79. doi:10.1016/j.matbio.2013.08.004. [PubMed: 24001398]

[2]. Iozzo RV, Basement membrane proteoglycans: from cellar to ceiling, Nat. Rev. Mol. Cell Biol 6 (2005) 646–656. doi:10.1038/nrm1702. [PubMed: 16064139]

[3]. Iozzo RV, Perlecan: A gem of a proteoglycan, Matrix Biol 14 (1994) 203–208. doi: 10.1016/0945-053X(94)90183-X. [PubMed: 7921536]

[4]. Grindel BJ, Martinez JR, V Tellman T, Harrington DA, Zafar H, Nakhleh L, Chung LW, Farach-Carson MC, Matrilysin/MMP-7 Cleavage of Perlecan/HSPG2 Complexed with Semaphorin 3A Supports FAK-Mediated Stromal Invasion by Prostate Cancer Cells, Sci. Rep 8 (2018) 7262. doi: 10.1038/s41598-018-25435-3. [PubMed: 29740048]

[5]. Thompson WR, Modla S, Grindel BJ, Czymmek KJ, Kirn-Safran CB, Wang L, Duncan RL, Farach-Carson MC, Perlecan/Hspg2 deficiency alters the pericellular space of the lacunocanalicular system surrounding osteocytic processes in cortical bone, J. Bone Miner. Res 26 (2011) 618–629. doi:10.1002/jbmr.236. [PubMed: 20814969]

[6]. Rodgers KD, Sasaki T, Aszodi A, Jacenko O, Reduced perlecan in mice results in chondrodysplasia resembling Schwartz–Jampel syndrome, Hum. Mol. Genet 16 (2007) 515–528. doi:10.1093/hmg/ddl484. [PubMed: 17213231]

[7]. Arikawa-Hirasawa E, Le AH, Nishino I, Nonaka I, Ho NC, Francomano CA, Govindraj P, Hassell JR, Devaney JM, Spranger J, Stevenson RE, Iannaccone S, Dalakas MC, Yamada Y, Structural and Functional Mutations of the Perlecan Gene Cause Schwartz-Jampel Syndrome, with Myotonic Myopathy and Chondrodysplasia, Am. J. Hum. Genet 70 (2002) 1368–1375. doi: 10.1086/340390. [PubMed: 11941538]

[8]. Stum M, Davoine C-S, Vicart S, Guillot-Noël L, Topaloglu H, Carod-Artal FJ, Kayserili H, Hentati F, Merlini L, Urtizberea JA, Hammouda E-H, Quan PC, Fontaine B, Nicole S, Spectrum of HSPG2 (Perlecan) mutations in patients with Schwartz-Jampel syndrome, Hum. Mutat 27 (2006) 1082–1091. doi:10.1002/humu.20388. [PubMed: 16927315]

[9]. Lowe DA, Lepori-Bui N, Fomin PV, Sloofman LG, Zhou X, Farach-Carson MC, Wang L, Kirn-Safran CB, Deficiency in Perlecan/HSPG2 During Bone Development Enhances Osteogenesis and Decreases Quality of Adult Bone in Mice, Calcif. Tissue Int 95 (2014) 29–38. doi:10.1007/s00223-014-9859-2. [PubMed: 24798737]

[10]. Wang B, Lai X, Price C, Thompson WR, Li W, Quabili TR, Tseng W-J, Liu XS, Zhang H, Pan J, Kirn-Safran CB, Farach-Carson MC, Wang L, Perlecan-Containing Pericellular Matrix Regulates Solute Transport and Mechanosensing Within the Osteocyte Lacunar-Canalicular System, J. Bone Miner. Res 29 (2014) 878–891. doi:10.1002/jbmr.2105. [PubMed: 24115222]

[11]. Huiskes R, Ruimerman R, van Lenthe GH, Janssen JD, Effects of mechanical forces on maintenance and adaptation of form in trabecular bone, Nature. 405 (2000) 704–706. doi: 10.1038/35015116. [PubMed: 10864330]

[12]. Aarden EM, Burger EH, Nijweide PJ, Function of osteocytes in bone., J. Cell. Biochem 55 (1994) 287–99. doi:10.1002/jcb.240550304. [PubMed: 7962159]

[13]. Wang L, Solute Transport in the Bone Lacunar-Canalicular System (LCS), Curr. Osteoporos. Rep 16 (2018) 32–41. doi:10.1007/s11914-018-0414-3. [PubMed: 29349685]

[14]. Wijeratne SS, Martinez JR, Grindel BJ, Frey EW, Li J, Wang L, Farach-Carson MC, Kiang C-H, Single molecule force measurements of perlecan/HSPG2: A key component of the osteocyte pericellular matrix, Matrix Biol 50 (2016) 27–38. doi:10.1016/j.matbio.2015.11.001. [PubMed: 26546708]

[15]. You L-D, Weinbaum S, Cowin SC, Schaffler MB, Ultrastructure of the osteocyte process and its pericellular matrix, Anat. Rec 278A (2004) 505–513. doi:10.1002/ar.a.20050.

[16]. Wang B, Zhou X, Price C, Li W, Pan J, Wang L, Quantifying load-induced solute transport and solute-matrix interaction within the osteocyte lacunar-canalicular system, J. Bone Miner. Res 28 (2013) 1075–1086. doi:10.1002/jbmr.1804. [PubMed: 23109140]

[17]. Qin Y-X, Kaplan T, Saldanha A, Rubin C, Fluid pressure gradients, arising from oscillations in intramedullary pressure, is correlated with the formation of bone and inhibition of intracortical porosity, J. Biomech 36 (2003) 1427–1437. doi:10.1016/S0021-9290(03)00127-1. [PubMed: 14499292]

[18]. Kwon RY, Meays DR, Tang WJ, Frangos JA, Microfluidic enhancement of intramedullary pressure increases interstitial fluid flow and inhibits bone loss in hindlimb suspended mice, J. Bone Miner. Res 25 (2010) 1798–1807. doi:10.1002/jbmr.74. [PubMed: 20200992]

[19]. Hu M, Cheng J, Bethel N, Serra-Hsu F, Ferreri S, Lin L, Qin Y-X, Interrelation between external oscillatory muscle coupling amplitude and in vivo intramedullary pressure related bone adaptation, Bone. 66 (2014) 178–181. doi:10.1016/j.bone.2014.05.018. [PubMed: 24947450]

[20]. Kwon RY, Meays DR, Meilan AS, Jones J, Miramontes R, Kardos N, Yeh J-C, Frangos JA, Skeletal Adaptation to Intramedullary Pressure-Induced Interstitial Fluid Flow Is Enhanced in Mice Subjected to Targeted Osteocyte Ablation, PLoS One. 7 (2012) e33336. doi:10.1371/journal.pone.0033336. [PubMed: 22413015]

[21]. Curtis KJ, Coughlin TR, Mason DE, Boerckel JD, Niebur GL, Bone marrow mechanotransduction in porcine explants alters kinase activation and enhances trabecular bone formation in the absence of osteocyte signaling, Bone. 107 (2018) 78–87. doi:10.1016/j.bone.2017.11.007. [PubMed: 29154967]

[22]. Metzger TA, Kreipke TC, Vaughan TJ, McNamara LM, Niebur GL, The In Situ Mechanics of Trabecular Bone Marrow: The Potential for Mechanobiological Response, J. Biomech. Eng 137 (2015) 1–7. doi:10.1115/1.4028985.

[23]. Kim CH, Kim KH, Jacobs CR, Effects of high frequency loading on RANKL and OPG mRNA expression in ST-2 murine stromal cells, BMC Musculoskelet. Disord 10 (2009) 109. doi:10.1186/1471-2474-10-109. [PubMed: 19728893]

[24]. McAllister TN, Du T, Frangos JA, Fluid Shear Stress Stimulates Prostaglandin and Nitric Oxide Release in Bone Marrow-Derived Preosteoclast-like Cells, Biochem. Biophys. Res. Commun 270 (2000) 643–648. doi:10.1006/bbrc.2000.2467. [PubMed: 10753677]

[25]. Bratengeier C, Bakker AD, Fahlgren A, Mechanical loading releases osteoclastogenesis-modulating factors through stimulation of the P2X7 receptor in hematopoietic progenitor cells, J. Cell. Physiol 234 (2019) 13057–13067. doi:10.1002/jcp.27976. [PubMed: 30536959]

[26]. Duncan RL, Turner CH, Mechanotransduction and the functional response of bone to mechanical strain, Calcif. Tissue Int 57 (1995) 344–358. doi:10.1007/BF00302070. [PubMed: 8564797]

[27]. Thompson WR, Rubin CT, Rubin J, Mechanical regulation of signaling pathways in bone, Gene. 503 (2012) 179–193. doi:10.1016/j.gene.2012.04.076. [PubMed: 22575727]

[28]. Dallas SL, Prideaux M, Bonewald LF, The Osteocyte: An Endocrine Cell … and More, Endocr. Rev 34 (2013) 658–690. doi:10.1210/er.2012-1026. [PubMed: 23612223]

[29]. Kelly NH, Schimenti JC, Ross FP, van der Meulen MCH, Transcriptional profiling of cortical versus cancellous bone from mechanically-loaded murine tibiae reveals differential gene expression, Bone. 86 (2016) 22–29. doi:10.1016/j.bone.2016.02.007. [PubMed: 26876048]

[30]. Wang B, Du T, Wang Y, Yang C, Zhang S, Cao X, Focal adhesion kinase signaling pathway is involved in mechanotransduction in MG-63 Cells, Biochem. Biophys. Res. Commun 410 (2011) 671–676. doi:10.1016/j.bbrc.2011.06.054. [PubMed: 21693107]

[31]. Watabe H, Furuhama T, Tani-Ishii N, Mikuni-Takagaki Y, Mechanotransduction activates α5β1 integrin and PI3K/Akt signaling pathways in mandibular osteoblasts, Exp. Cell Res 317 (2011) 2642–2649. doi:10.1016/j.yexcr.2011.07.015. [PubMed: 21824471]

[32]. Robinson JA, Chatterjee-Kishore M, Yaworsky PJ, Cullen DM, Zhao W, Li C, Kharode Y, Sauter L, Babij P, Brown EL, Hill AA, Akhter MP, Johnson ML, Recker RR, Komm BS, Bex FJ, Wnt/β-Catenin Signaling Is a Normal Physiological Response to Mechanical Loading in Bone, J. Biol. Chem 281 (2006) 31720–31728. doi:10.1074/jbc.M602308200. [PubMed: 16908522]

[33]. Lu XL, Huo B, Chiang V, Guo XE, Osteocytic network is more responsive in calcium signaling than osteoblastic network under fluid flow, J. Bone Miner. Res 27 (2012) 563–574. doi:10.1002/jbmr.1474. [PubMed: 22113822]

[34]. Jing D, Baik AD, Lu XL, Zhou B, Lai X, Wang L, Luo E, Guo XE, In situ intracellular calcium oscillations in osteocytes in intact mouse long bones under dynamic mechanical loading, FASEB J 28 (2014) 1582–1592. doi:10.1096/fj.13-237578. [PubMed: 24347610]

[35]. Ypey DL, Weidema AF, Höld KM, Van Der Laarse A, Ravesloot JH, Van Der Plas A, Nijweide PJ, Voltage, calcium, and stretch activated ionic channels and intracellular calcium in bone cells, J. Bone Miner. Res 7 (1992) S377–S387. doi:10.1002/jbmr.5650071404. [PubMed: 1283043]

[36]. Jacobs CR, Yellowley CE, Davis BR, Zhou Z, Cimbala JM, Donahue HJ, Differential effect of steady versus oscillating flow on bone cells, J. Biomech 31 (1998) 969–976. doi:10.1016/S0021-9290(98)00114-6. [PubMed: 9880053]

[37]. Li YJ, Batra NN, You L, Meier SC, Coe IA, Yellowley CE, Jacobs CR, Oscillatory fluid flow affects human marrow stromal cell proliferation and differentiation, J. Orthop. Res 22 (2004) 1283–1289. doi:10.1016/j.orthres.2004.04.002. [PubMed: 15475210]

[38]. Berridge MJ, Lipp P, Bootman MD, The versatility and universality of calcium signalling, Nat. Rev. Mol. Cell Biol 1 (2000) 11–21. doi:10.1038/35036035. [PubMed: 11413485]

[39]. Ayturk UM, Jacobsen CM, Christodoulou DC, Gorham J, Seidman JG, Seidman CE, Robling AG, Warman ML, An RNA-seq protocol to identify mRNA expression changes in mouse diaphyseal bone: Applications in mice with bone property altering Lrp5 mutations, J. Bone Miner. Res 28 (2013) 2081–2093. doi:10.1002/jbmr.1946. [PubMed: 23553928]

[40]. Price C, Zhou X, Li W, Wang L, Real-time measurement of solute transport within the lacunar-canalicular system of mechanically loaded bone: Direct evidence for load-induced fluid flow, J. Bone Miner. Res 26 (2011) 277–285. doi:10.1002/jbmr.211. [PubMed: 20715178]

[41]. Burr DB, Milgrom C, Fyhrie D, Forwood M, Nyska M, Finestone A, Hoshaw S, Saiag E, Simkin A, In vivo measurement of human tibial strains during vigorous activity, Bone. 18 (1996) 405–410. doi:10.1016/8756-3282(96)00028-2. [PubMed: 8739897]

[42]. Lun ATL, Chen Y, Smyth GK, It's DE-licious: A Recipe for Differential Expression Analyses of RNA-seq Experiments Using Quasi-Likelihood Methods in edgeR, in: Methods Mol. Biol, 2016: pp. 391–416. doi:10.1007/978-1-4939-3578-9_19.

[43]. Huang DW, Sherman BT, Lempicki RA, Bioinformatics enrichment tools: paths toward the comprehensive functional analysis of large gene lists, Nucleic Acids Res 37 (2009) 1–13. doi:10.1093/nar/gkn923. [PubMed: 19033363]

[44]. Huang DW, Sherman BT, a Lempicki R, Systematic and integrative analysis of large gene lists using DAVID bioinformatics resources, Nat. Protoc 4 (2009) 44–57. doi:10.1038/nprot.2008.211. [PubMed: 19131956]

[45]. Babu GJ, Periasamy M, Transgenic mouse models for cardiac dysfunction by a specific gene manipulation., Methods Mol. Med 112 (2005) 365–77. http://www.ncbi.nlm.nih.gov/pubmed/16010030. [PubMed: 16010030]

[46]. Berridge MJ, Bootman MD, Roderick HL, Calcium signalling: dynamics, homeostasis and remodelling, Nat. Rev. Mol. Cell Biol 4 (2003) 517–529. doi:10.1038/nrm1155. [PubMed: 12838335]

[47]. Thompson WR, Perlecan modulates the function of the osteocyte lacuno-canalicular system, University of Delaware, 2011 https://search.proquest.com/docview/854508860/abstract/BFD510F4894D4BE3PQ/1?accountid=10457 (accessed March 21, 2019).

[48]. Brown GN, Leong PL, Guo XE, T-Type voltage-sensitive calcium channels mediate mechanically-induced intracellular calcium oscillations in osteocytes by regulating endoplasmic reticulum calcium dynamics, Bone. 88 (2016) 56–63. doi:10.1016/j.bone.2016.04.018. [PubMed: 27108342]

[49]. Thompson WR, Majid AS, Czymmek KJ, Ruff AL, García J, Duncan RL, Farach-Carson MC, Association of the α2δ1 subunit with Cav3.2 enhances membrane expression and regulates mechanically induced ATP release in MLO-Y4 osteocytes, J. Bone Miner. Res 26 (2011) 2125–2139. doi:10.1002/jbmr.437. [PubMed: 21638318]

[50]. Knaus HG, Scheffauer F, Romanin C, Schindler HG, Glossmann H, Heparin binds with high affinity to voltage-dependent L-type Ca2+ channels. Evidence for an agonistic action., J. Biol. Chem 265 (1990) 11156–66. http://www.ncbi.nlm.nih.gov/pubmed/2162834. [PubMed: 2162834]

[51]. Lacinova L, Cleemann L, Morad M, Ca2+ channel modulating effects of heparin in mammalian cardiac myocytes., J. Physiol 465 (1993) 181–201. doi:10.1113/jphysiol.1993.sp019672. [PubMed: 8229833]

[52]. Martínez M, García MC, Farías JM, Cruzblanca H, Sánchez JA, Modulation of Ca2+ channels, charge movement and Ca2+ transients by heparin in frog skeletal muscle fibres., J. Muscle Res. Cell Motil 17 (1996) 575–94. doi:10.1007/BF00124356. [PubMed: 8906624]

[53]. Bezprozvanny IB, Ondrias K, Kaftan E, Stoyanovsky DA, Ehrlich BE, Activation of the calcium release channel (ryanodine receptor) by heparin and other polyanions is calcium dependent., Mol. Biol. Cell 4 (1993) 347–52. doi:10.1091/mbc.4.3.347. [PubMed: 7683508]

[54]. Ritov VB, Men'shikova EV, Kozlov YP, Heparin induces Ca 2+ release from the terminal cysterns of skeletal muscle sarcoplasmic reticulum, FEBS Lett 188 (1985) 77–80. doi: 10.1016/0014-5793(85)80878-4. [PubMed: 2410295]

[55]. Jenniskens GJ, Ringvall M, Koopman WJH, Ledin J, Kjellén L, Willems PHGM, Forsberg E, Veerkamp JH, van Kuppevelt TH, Disturbed Ca2+ kinetics in N-deacetylase/N-sulfotransferase-1 defective myotubes., J. Cell Sci 116 (2003) 2187–93. doi:10.1242/jcs.00447. [PubMed: 12692154]

[56]. Shao Y, Alicknavitch M, Farach-Carson MC, Expression of voltage sensitive calcium channel (VSCC) L-type Cav1.2 (α1C) and T-type Cav3.2 (α1H) subunits during mouse bone development, Dev. Dyn 234 (2005) 54–62. doi:10.1002/dvdy.20517. [PubMed: 16059921]

[57]. Bergh JJ, Shao Y, Puente E, Duncan RL, Farach-Carson MC, Osteoblast Ca 2+ permeability and voltage-sensitive Ca 2+ channel expression is temporally regulated by 1,25-dihydroxyvitamin D 3, Am. J. Physiol. Physiol 290 (2006) C822–C831. doi:10.1152/ajpcell.00403.2005.

[58]. Nencini S, Ivanusic J, Mechanically sensitive Aδ nociceptors that innervate bone marrow respond to changes in intra-osseous pressure, J. Physiol 595 (2017) 4399–4415. doi:10.1113/JP273877. [PubMed: 28295390]

[59]. Guilak F, Leddy HA, Liedtke W, Transient receptor potential vanilloid 4: The sixth sense of the musculoskeletal system?, Ann. N. Y. Acad. Sci 1192 (2010) 404–9. doi:10.1111/j. 1749-6632.2010.05389.x. [PubMed: 20392266]

[60]. Mantila Roosa SM, Turner CH, Liu Y, Regulatory mechanisms in bone following mechanical loading., Gene Regul. Syst. Bio 6 (2012) 43–53. doi:10.4137/GRSB.S8068.

[61]. Wasserman E, Webster D, Kuhn G, Attar-Namdar M, Müller R, Bab I, Differential load-regulated global gene expression in mouse trabecular osteocytes., Bone. 53 (2013) 14–23. doi:10.1016/ j.bone.2012.11.017. [PubMed: 23201221]

[62]. Govey PM, Kawasawa YI, Donahue HJ, Mapping the osteocytic cell response to fluid flow using RNA-Seq., J. Biomech 48 (2015) 4327–32. doi:10.1016/j.jbiomech.2015.10.045. [PubMed: 26573903]

[63]. Robling AG, Niziolek PJ, Baldridge LA, Condon KW, Allen MR, Alam I, Mantila SM, Gluhak-Heinrich J, Bellido TM, Harris SE, Turner CH, Mechanical stimulation of bone in vivo reduces osteocyte expression of Sost/sclerostin., J. Biol. Chem 283 (2008) 5866–75. doi:10.1074/ jbc.M705092200. [PubMed: 18089564]

[64]. Tu X, Rhee Y, Condon KW, Bivi N, Allen MR, Dwyer D, Stolina M, Turner CH, Robling AG, Plotkin LI, Bellido T, Sost downregulation and local Wnt signaling are required for the osteogenic response to mechanical loading., Bone. 50 (2012) 209–17. doi:10.1016/j.bone. 2011.10.025. [PubMed: 22075208]

[65]. Lara-Castillo N, Kim-Weroha NA, Kamel MA, Javaheri B, Ellies DL, Krumlauf RE, Thiagarajan G, Johnson ML, In vivo mechanical loading rapidly activates β-catenin signaling in osteocytes through a prostaglandin mediated mechanism., Bone. 76 (2015) 58–66. doi:10.1016/j.bone. 2015.03.019. [PubMed: 25836764]

[66]. Ko FC, Dragomir C, Plumb DA, Goldring SR, Wright TM, Goldring MB, van der Meulen MCH, In vivo cyclic compression causes cartilage degeneration and subchondral bone changes in mouse tibiae., Arthritis Rheum 65 (2013) 1569–78. doi:10.1002/art.37906. [PubMed: 23436303]

[67]. Srinivasan PP, Parajuli A, Price C, Wang L, Duncan RL, Kirn-Safran CB, Inhibition of T-Type Voltage Sensitive Calcium Channel Reduces Load-Induced OA in Mice and Suppresses the

Catabolic Effect of Bone Mechanical Stress on Chondrocytes., PLoS One. 10 (2015) e0127290. doi:10.1371/journal.pone.0127290. [PubMed: 26011709]

Highlights

- Perlecan deficiency impairs osteocytes' intracellular calcium response to loading
- Perlecan deficiency suppresses ER calcium regulators in loaded bone
- Perlecan deficiency blunts the activation of signaling pathways induced by loading
- Repetitive 7-day loading induces broader transcriptome changes than 1-day loading

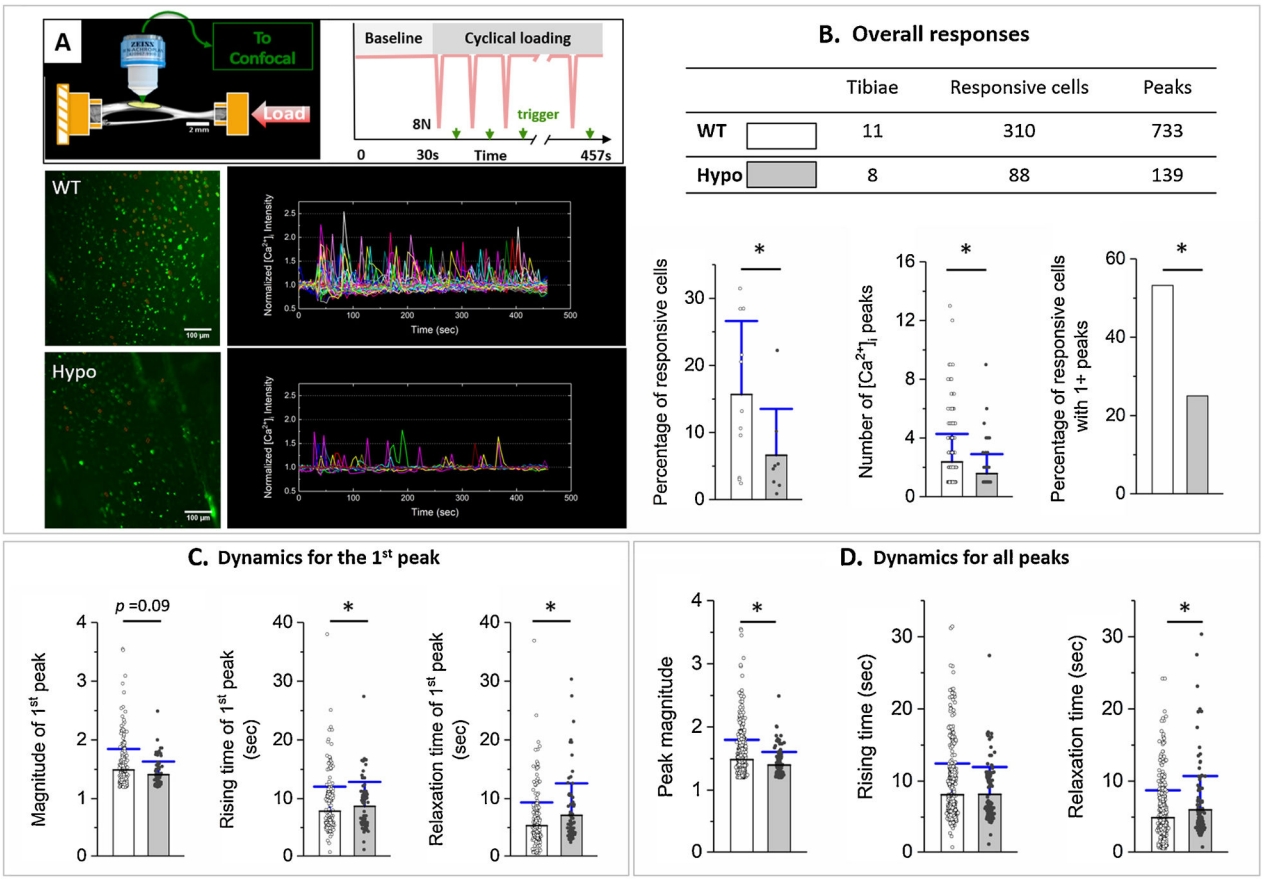

Figure 1.

Osteocytes of Hypo murine tibiae showed impaired intracellular calcium $[Ca^{2+}]_i$ response to mechanical loading. (A) Freshly dissected murine tibiae were subjected to axial cyclic loading (8 N peak load), and intracellular calcium $[Ca^{2+}]_i$ of osteocytes beneath the anterior-medial surface were imaged using confocal microscopy and trigger signals inserted between loading cycles. Representative images of osteocytes (green, left panel) and normalized $[Ca^{2+}]_i$ traces of individual cells (right panel) are shown for tests using WT and Hypo tibiae. (B) The overall responses included the percentage of responsive cells over the total number of cells, the number of $[Ca^{2+}]_i$ peaks (averaged for all responsive cells), and the percentage of responsive cells with multiple $[Ca^{2+}]_i$ peaks. (C) Dynamics for the first peak included the magnitude, rising time, and relaxation time. (D) Dynamics for all peaks included the magnitude, rising time, and relaxation time. Mean, standard deviation, and individual data points are shown. * indicates statistical significance $p < 0.05$ between WT and Hypo using Mann–Whitney U or Chi-square tests.

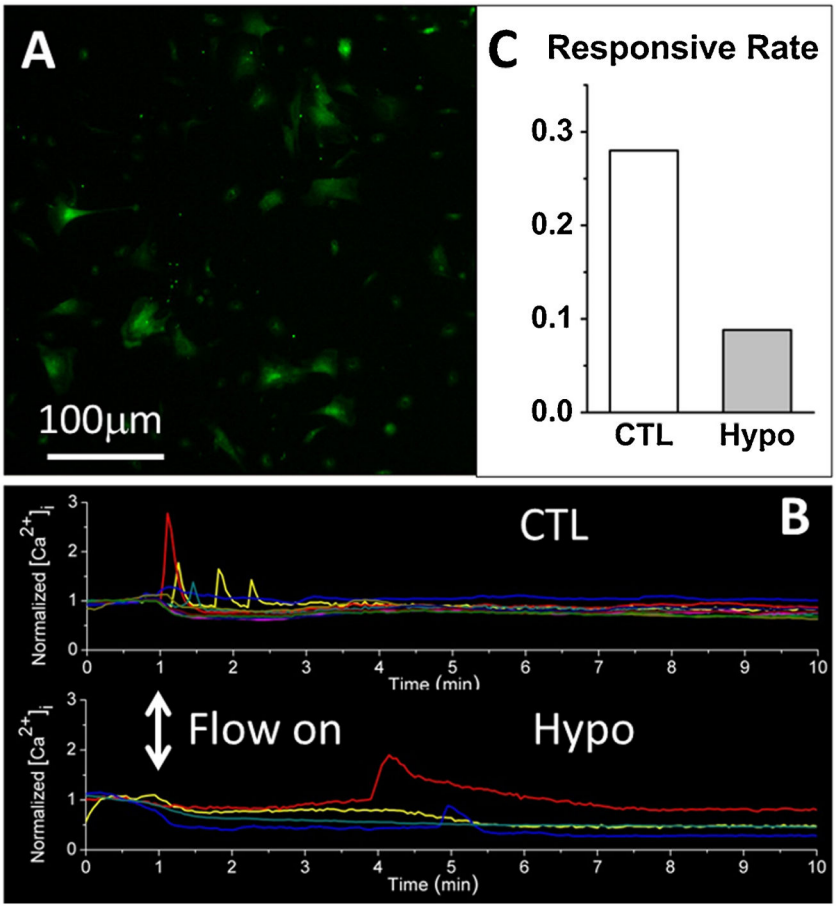

Figure 2.

Impaired $[Ca2+]_i$ response to fluid shear in primary MSC derived from Hypo bone marrow. (A) Both Hypo and wild type CTL MSCs showed a typical spindle-like shape. (B) Fewer Hypo MSCs exhibited $[Ca2+]_i$ peaks. (C) Relative to CTL, Hypo MSC showed three times reduction of responsive rate (0.088 vs. 0.28).

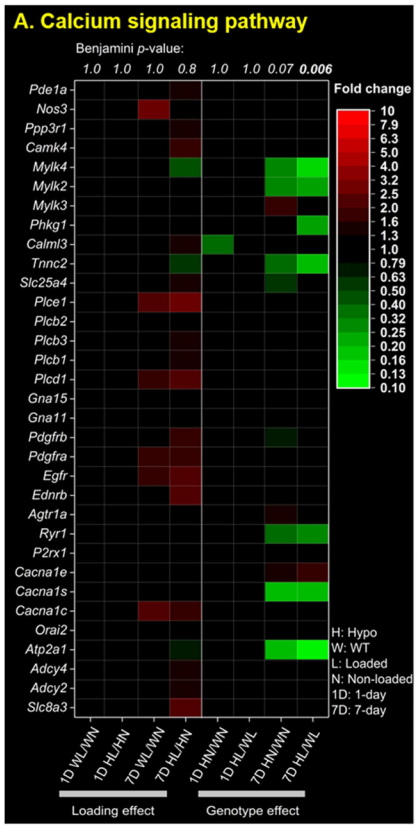

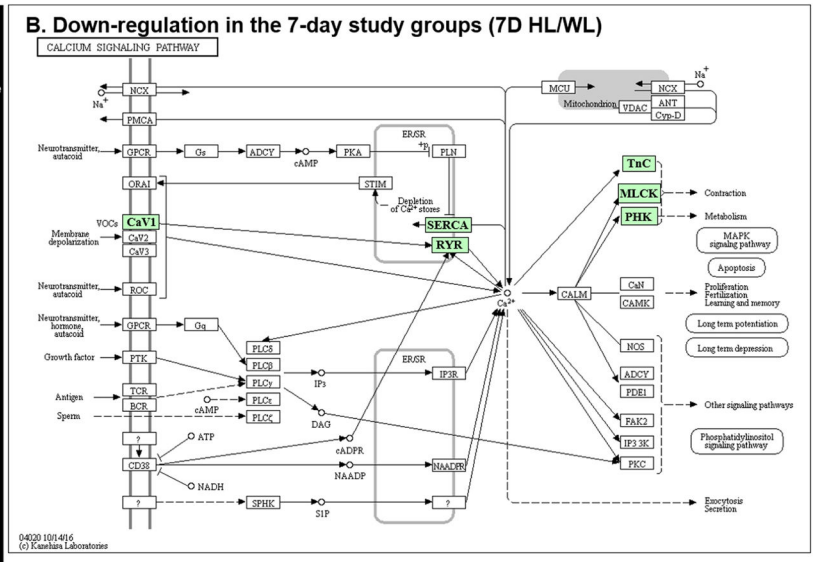

Transcript	WT (RPKM)	Hypo (RPKM)	F.C.
Cacna1s	0.30	0.05	0.17
Ryr1	0.50	0.13	0.26
Atp2a1/Serca	12.73	1.53	0.12
Tnnc2	13.90	2.40	0.17
Mylk4	0.33	0.05	0.14
Mylk2	0.88	0.20	0.23
Phkg1	0.29	0.06	0.21

C. RNA seq (7D HL/WL)

D. RT-PCR (/Gapdh)

Transcript	WT (ΔCT)	Hypo (ΔCT)	F.C
Ryr1	5.91	6.88	0.52
Atp2a1/Serca	3.45	4.10	0.71

Figure 3.

Effects of mechanical loading and perlecan deficiency on calcium signaling pathway revealed by RNA sequencing. (A) A heat map of fold changes (F.C.) of individual genes (red color: F.C. > 1; green color: F.C. > 1; black color: F.C. =1 or FDR > 0.05) for 8 comparisons between loaded (L) *vs.* non-loaded (N) tibiae from the same animals (loading effects) or the Hypo (H) *vs.* WT (W) tibiae under the same loading condition (genotype effects) following 1-day (1D) or 7-day (7D) loading. The significance level of pathway enrichment (Benjamini *p*–value) is given (top) and comparisons are indicated at the bottom of each column. (B). The calcium signaling pathway was suppressed for Hypo loaded bone relative to WT following 7-day loading, as highlighted by green boxes. (C) The expression level (RPKM) and fold change values of the seven DETs (7-day Hypo vs. WT loaded tibiae) annotated in the calcium signaling pathway. (D). Decreased transcripts in Hypo vs. WT of two key ER calcium cycling regulators (*Ryr1* and *Atp2a1*) were corroborated using qRT-PCR and *Gapdh* as the housekeeping gene.

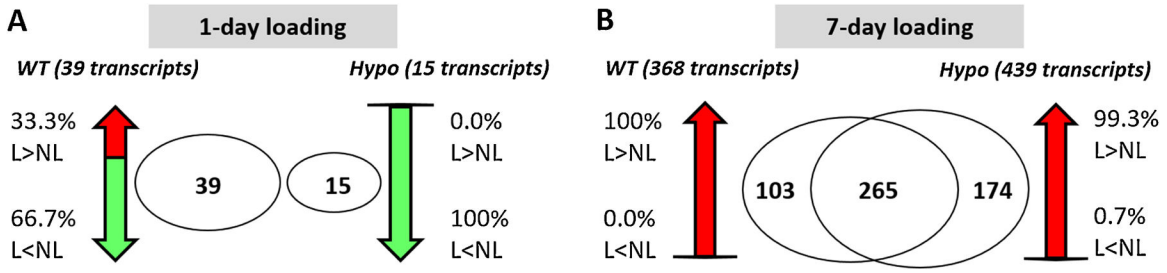

C. Enriched Pathway Analysis

Signaling Pathway	1-day WL/WN	1-day HL/HN	7-day WL/WN	7-day HL/HN
	# annotated DETs (# increased ↑, # decreased ↓) (Benjamini *p value*)			
ECM-receptor interaction	2 (1 ↑, 1 ↓) (p = 0.8)	0	25 (25 ↑, 0 ↓) **(p = 9x10^{-22})**	28 (28 ↑, 0 ↓) **(p = 2x10^{-23})**
Focal adhesion	2 (1 ↑, 1 ↓) (p = 0.9)	0	26 (26 ↑, 0 ↓) **(p = 5x10^{-14})**	33 (32 ↑, 1 ↓) **(p = 2x10^{-18})**
PI3K-Akt signaling	3 (1 ↑, 2 ↓) (p= 0.7)	0	28 (28 ↑, 0 ↓) **(p = 1x10^{-10})**	35 (35 ↑, 0 ↓) **(p = 1x10^{-13})**
Wnt signaling	0	0	4 (4 ↑, 0 ↓) (p = 0.9)	7 (7 ↑, 0 ↓) (p = 0.4)

Figure 4.

Transcriptome changes in WT and Hypo tibiae following mechanical loading. Venn diagrams show the number of DETs (loaded vs. non-loaded) and percentage of increased (↑; red color: F.C. > 2) or decreased (↓; green color: F.C. < 0.5) transcripts after (A) 1-day or (B) 7-day loading. (C). Enrichment analysis of four selected signaling pathways (ECM-receptor interaction, focal adhesion, PI3K-Akt, and Wnt signaling) following loading in WT and Hypo tibiae (Benjamini $p < 0.05$ indicates statistical significance). The first three pathways were enriched in both genotypes with high significance level after 7-day loading.

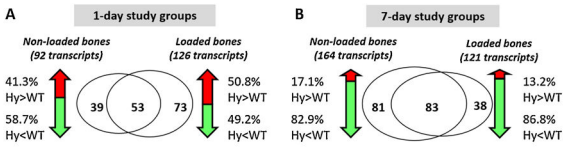

C. Enriched Pathway Analysis

Signaling Pathway	1-day HN/WN	1-day HL/WL	7-day HN/WN	7-day HL/WL
	# annotated DETs (# increased ↑, # decreased ↓) (Benjamini *p value*)			
ECM-receptor interaction	0	5 (0 ↑, 5 ↓) (***p* = 0.004**)	2 (0 ↑, 2 ↓) (*p* = 0.9)	3 (0 ↑, 3 ↓) (*p* = 0.3)
Focal adhesion	0	5 (1 ↑, 4 ↓) (***p* = 0.05**)	7 (0 ↑, 7 ↓) (***p* = 0.03**)	6 (0 ↑, 6 ↓) (***p* = 0.04**)
PI3K-Akt signaling	1 (0 ↑, 1 ↓) (*p* = 1.0)	4 (0 ↑, 4 ↓) (*p* = 0.6)	2 (0 ↑, 2 ↓) (*p* = 1.0)	2 (0 ↑, 2 ↓) (*p* = 1.0)
Wnt signaling	0	2 (0 ↑, 2 ↓) (*p* = 0.9)	1 (0 ↑, 1 ↓) (*p* = 1.0)	0

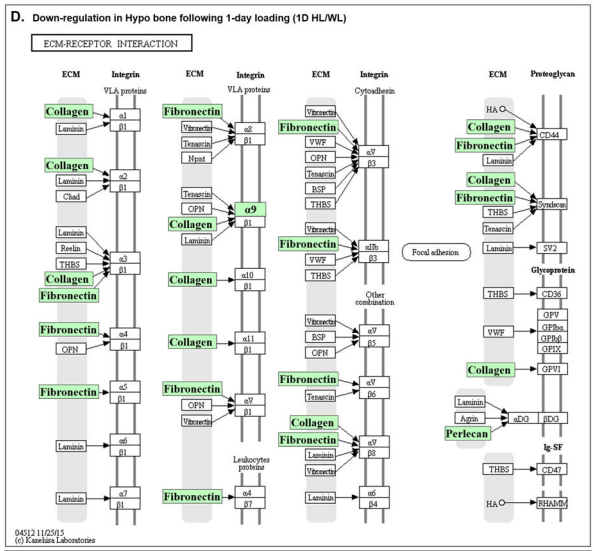

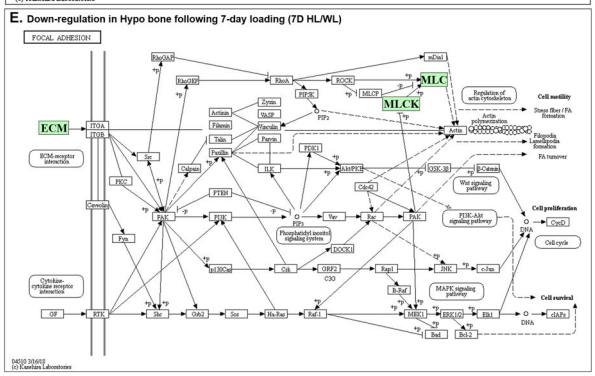

Figure 5.

The effects of perlecan deficiency on transcriptome changes in (A) the 1-day study groups and (B) the 7-day study groups. Venn diagrams show the number of DETs (Hypo vs. WT) and percentage of increased (red) or decreased (green) transcripts in both non-loaded and loaded bones. (C). Significant enrichment was found for ECM-receptor interaction and focal adhesion pathways in the cases of 1-day loaded (HL/WL) and/or 7-day non-loaded (HN/WN) and loaded (HL/WL) comparisons. (D) Suppression of ECM-receptor interaction pathway in Hypo bone following 1-day loading (1D HL/WL) was mainly due to decreased transcripts of ECM molecules. (E) Suppression of Focal adhesion pathway in Hypo bone following 7-day loading (7D HL/WL) was due to both decreased ECM and down-stream

MLCK and MLC gene/gene groups. Box color: red ↑(increased transcripts); green ↓ (decreased transcripts); white →(no change in transcript levels).

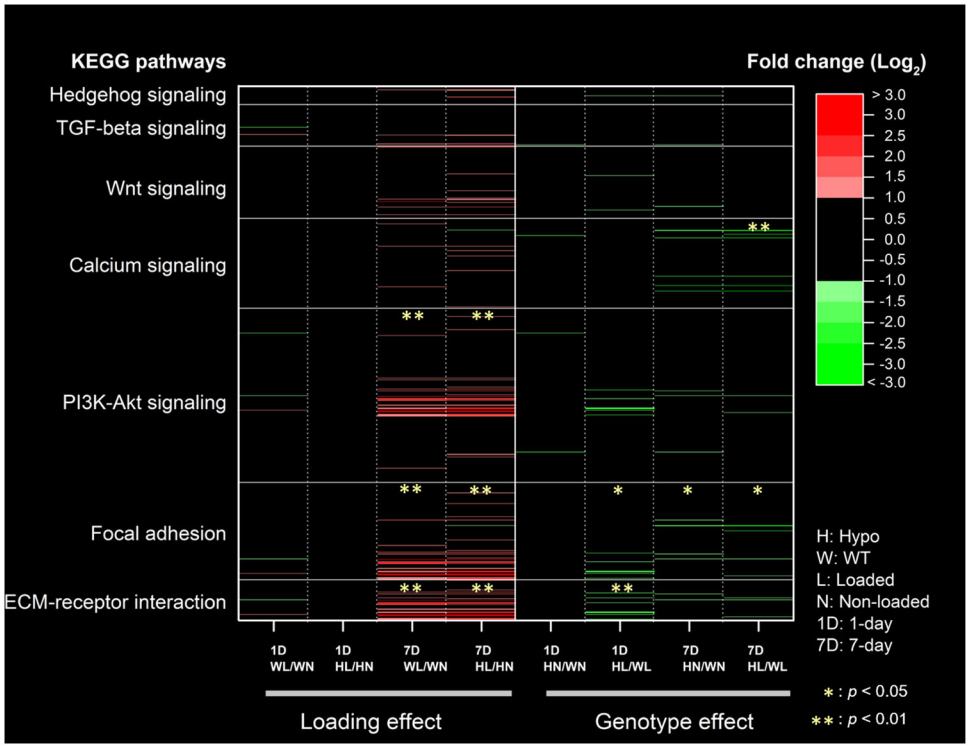

Figure 6.

The effects of mechanical loading and perlecan deficiency (genotype) on selective signaling pathways involved in mechanotransduction. Each row of the heat map represents a single gene product within the particular pathway and each column shows one comparison. Color and color intensity correspond to fold-change values. Comparison pairs are represented by loading duration 1-day (1D) or 7-day (7D), following by the two bones under comparison identified with genotype and loading condition (see keys on bottom right). Significantly enriched pathways are indicated by * ($p < 0.05$) or ** ($p < 0.01$) as assessed using Benjamini's test.